Size, shape, and flexibility of RNA structures

Changbong Hyeon[1] and Ruxandra I. Dima[2] and D. Thirumalai[1,3]

[1]Biophysics Program,

Institute for Physical Science and Technology,

University of Maryland,

College Park, MD 20742

[2]Department of Chemistry,

University of Cincinnati,

Cincinnati OH, 45221

[3]Department of Chemistry and Biochemistry,

University of Maryland,

College Park, MD 20742

(Dated: August 24, 2017)

Determination of sizes and flexibilities of RNA molecules is important in understanding the nature of packing in folded structures and in elucidating interactions between RNA and DNA or proteins. Using the coordinates of the structures of RNA in the Protein Data Bank we find that the size of the folded RNA structures, measured using the radius of gyration, R_G, follows the Flory scaling law, namely, $R_G = 5.5N^{1/3}$ Å where N is the number of nucleotides. The shape of RNA molecules is characterized by the asphericity Δ and the shape S parameters that are computed using the eigenvalues of the moment of inertia tensor. From the distribution of Δ, we find that a large fraction of folded RNA structures are aspherical and the distribution of S values shows that RNA molecules are prolate ($S > 0$). The flexibility of folded structures is characterized by the persistence length l_p. By fitting the distance distribution function, $P(r)$ that is computed using the coordinates of the folded RNA, to the worm-like chain model we extracted the persistence length l_p. We find that $l_p \approx 1.5N^{0.33}$ Å which might reflect the large separation between the free energies that stabilize secondary and tertiary structures. The dependence of l_p

on N implies the average length of helices should increases as the size of RNA grows. We also analyze packing in the structures of ribosomes (30S, 50S, and 70S) in terms of R_G, Δ, S, and l_p. The 70S and the 50S subunits are more spherical compared to most RNA molecules. The globularity in 50S is due to the presence of an unusually large number (compared to 30S subunit) of small helices that are stitched together by bulges and loops. Comparison of the shapes of the intact 70S ribosome and the constituent particles suggests that folding of the individual molecules might occur prior to assembly.

INTRODUCTION

Molecular recognition between RNAs or RNA and protein is involved in a number of cellular functions. In all these processes RNA interacts with other biomolecules. In order to understand the biophysical basis of interactions of RNA with other biological molecules it is necessary to characterize the shapes of the interacting partners. Hence, it is important to elucidate the shapes and flexibilities of RNA structures. The large increase in the number of three dimensional structures allows us to quantify RNA shapes which is needed to describe the assembly of complexes such as the ribosome.

In contrast to the situation in RNA much is known about packing and shape fluctuations in proteins.[1,2,3,4] In part this is because the number of solved protein structures is ∼30,000 while the RNA structure database contains only ∼600 structures. Despite considerable success in the secondary structure predictions of nucleic acid sequences using energy minimization dynamic programming algorithm[5,6] or comparative sequence analysis[7] the complicated nature of counterion-mediated tertiary interactions in RNAs makes it difficult to obtain three dimensional RNA structures using computational methods. The recent experimental determination of medium to large size of RNA structures has prompted us to perform a statistical analysis of RNA structures with the aim of characterizing their shapes and flexibility.

In this paper, we study the structural features of RNA using the currently available RNA three dimensional structures.[8] The size of RNA, as measured by the radius of gyration R_G, shows that typically RNA molecules are compact. The variation of R_G with the number (N) of nucleotides obeys Flory law i.e., $R_G = aN^{1/3}$ Å. Although the overall scaling law for R_G for RNA is identical to that for proteins there are considerable differences in their shapes. We find that the folded states of RNAs are largely prolate and are considerably more aspherical than

proteins. The flexibility of RNA, which is crucial in describing interactions with proteins and RNA and DNA, is described in terms of the persistence length (l_p) which can be measured using X-ray scattering[9] and other methods.[10] The values of l_p for RNA, which are considerably larger than for proteins, vary between (5-30)Å depending on N. Using the shape parameters and l_p we also describe the unusual structural characteristics of the ribosome, a large ribonucleoprotein complex.

METHODS

RNA structures : We computed several quantities to characterize the shapes of RNA using the atomic coordinates of their structures determined by X-ray crystallography, NMR, or cryo-EM. The coordinates for all RNA structures were obtained from the Protein Data Bank (PDB).[8] Our analysis is performed for over 1185 individual RNA chains with the number of nucleotides $N > 10$ found in 642 RNA related PDB files as of June 2005. Among these, 195 RNA chain structures are monomers, and the rest of the chains are part of oligomers or appear in complexes with other RNA molecules or proteins. Structural features in the monomeric form can be different from those determined in an oligomer or complex because the intermolecular interaction can affect the individual chain structure. Therefore, we analyzed the two groups of structures separately. For comparison, we have also calculated shape characteristics for a dataset of proteins. The results for proteins enable us to assess certain unusual features of RNA-protein interactions especially in the ribosome.

Size : The radius of gyration (R_G) is an indicator of the overall size of RNA. The value of R_G^2, which can be measured using small angle X-ray or neutron scattering, is calculated using

$$R_G^2 = \frac{1}{2\sum_i^M m_i \sum_j^M m_j N^2} \sum_i^M \sum_j^M m_i m_j (\vec{r}_i - \vec{r}_j)^2. \quad (1)$$

where M is the number of atoms in the molecule, and m_i is the mass of the i^{th} atom. In the calculation of R_G^2 for RNA structure we used only the coordinates of the heavy atoms (C, N, O, P).

Shape : The deviation from the spherical shape is characterized by the asphericity Δ and

the shape parameter S, both of which are calculated from the inertia tensor,[11,12]

$$\begin{aligned}\mathcal{T}_{\alpha\beta} &= \frac{1}{2\sum_i^M m_i \sum_j^M m_j}\sum_i^M\sum_j^M m_i m_j (r_{i\alpha}-r_{j\alpha})(r_{i\beta}-r_{j\beta}) \\ &= \frac{1}{\sum_i^M m_i}\sum_i^M m_i (r_{i\alpha}-R_{C\alpha})(r_{i\beta}-R_{C\beta}) \end{aligned} \quad (2)$$

where $r_{i\alpha}$ is the α-th Cartesian component of the position of atom i, and $\vec{R}_C = \sum_i^M m_i\vec{r}_i/\sum_i^M m_i$ is the a center of mass. The square of the radius of gyration is $R_G^2 = tr\mathcal{T}$. The eigenvalues λ_1, λ_2 and λ_3 of the matrix $\mathcal{T}$ are the the squares of the three principal radii of gyration. The extent of asphericity is characterized using Δ ($0 \le \Delta \le 1$)

$$\Delta = \frac{3}{2}\frac{\sum_{i=1}^3(\lambda_i-\overline{\lambda})^2}{(tr\mathcal{T})^2} \quad (3)$$

where $\overline{\lambda} = (\lambda_1+\lambda_2+\lambda_3)/3$. For a perfect sphere $\Delta = 0$. Deviation from $\Delta = 0$ indicates the extent of anisotropy. The overall shape of a molecule is assessed using

$$S = 27\frac{\prod_{i=1}^3(\lambda_i-\overline{\lambda})}{(tr\mathcal{T})^3} \quad (4)$$

which satisfies the bound $-1/4 \le S \le 2$. Negative values of S correspond to oblate ellipsoids and $S > 0$ are prolate ellipsoids.

Most studies of packing in proteins and RNAs involve tessellation of space which always introduces certain amount of arbitrariness.[4,13] In contrast, the shape parameters Δ and S are directly computed using only the atomic coordinates. Knowledges of Δ and S are important in determining the overall motion of RNA and their interaction with other biomolecules.

Persistence Length : A parameter that describes the flexibility of biomolecules is the persistence length, l_p, which is most clearly defined by assuming that RNA structures can be described by a polymer model. Based on previous experimental studies it is suspected that the statistical properties of dsDNA,[10,14] ssDNA,[15] and RNA[9,16] can be described using the worm-like chain (WLC) model. For WLC models l_p can be estimated provided the distribution of the mean end-to-end distance R_E or R_G is known. Exact calculation of neither $P(R_E)$ nor $P(R_G)$ is possible for WLC. A simple and accurate theoretical expression has been derived for $P(R_E)$ of worm-like chain using the mean field approximation.[17,18] The resulting distribution, which is in good agreement with computer simulations,[19] is

$$P_{WLC}(r_E) = \frac{4\pi C r_E^2}{(1-r_E^2)^{9/2}}\exp[-\frac{3t}{4(1-r_E^2)}]. \quad (5)$$

where $r_E \equiv R_E/L$ and $t \equiv L/l_p$. L is the contour length. For RNA molecules, which from the perspective of polymers, can be viewed as a branched polyelectrolyte chains, the contour length is also an unknown parameter. The normalization constant $C = 1/[\pi^{3/2}e^{-\alpha}\alpha^{-3/2}(1 + 3\alpha^{-1} + 15/4\alpha^{-2})]$ with an $\alpha = 3t/4$. When l_p is small $P_{WLC}(r_E)$ reduces to a Gaussian chain whereas for large l_p $P_{WLC}(r_E)$ approaches the rod-limit as $r_E \to 1$.

Although direct measurements of $P(R_E)$ for biomolecules are not routinely performed it is conceivable that $P(R_E)$ may be obtained using single molecule FRET experiments. However, the distance distribution function $P(r)$ can be measured using SAXS experiments.[20,21,22] Based on general arguments, we expect that the distribution functions $P(r)$ and $P(R_E)$ should coincide provided $r \gg R_G$. Because $\langle R_E^2 \rangle \sim \langle R_G^2 \rangle \sim Ll_p$ for WLC provided L is large it follows scaling arguments that $P(r)$ should decay for large r as

$$P(r) = \beta \exp\left(-\frac{1}{1-x^2}\right) \tag{6}$$

where $x = l_p r/R_G^2$, and β is an arbitrary constant. In practice Eq.6 accurately describes $P(r)$ computed using the coordinates of RNA structures when $r/R_g > 1$. We determined l_p by fitting the $P(r)$ function for RNA structures to Eq.6.

Recently, we used Eq.6 to analyze small angle X-ray scattering data. We showed that l_p for the Azoarcus ribozyme changes by a factor of 2 as the molecule folds upon addition of counterions (Mg^{2+} or Na^{+}). Although the structural basis for the success of WLC in describing certain properties of folded RNA is unclear, Eq.6 is useful in analyzing scattering data.

For purposes of comparisons we have also calculated $P(r)$ for folded structures for 56,000 protein chains. To our knowledge the persistence length of proteins has not been directly measured. We obtain l_p by fitting $P(r)$, obtained from the coordinates of the structures in the PDB, to Eq.6.

RESULTS

Distribution of RNA structures as a function of N: From the distribution of $P(N)$ the number of RNA structures in the PDB as a function of chain length (N) in Fig.1 we find that $\sim 70\%$ of the database contains N in the range $10 < N < 30$. The peak in $P(N)$ between $70 < N < 80$ is due to the large number of tRNA structures that have been determined in various conditions. The peaks at $N \approx 1500$ and $N \approx 3000$ correspond to 16S and 23S ribosomal RNAs, respectively. Compared to statistics of protein structures (see Fig.1 inset), RNA structures are more clustered at small values of N but span a broader range of N. However, this distribution is unrelated to the number of RNA molecules that are relevant to biological

functions. There is a broad range in N that represents noncoding RNAs. For example, the length of human ncRNA functioning in gene silencing process is ∼100,000 nucleotides.[23] From Fig.1, which reflects the current status in RNA structure determination, it is clear that there is a large gap between the total number of functional RNAs and those with known three dimensional structures.

Size of RNA obeys the Flory law : If the overall shape of RNA is spherical then its volume, an extensive variable, is $V \approx \frac{4\pi}{3} R_G^3$ with R_G being the radius of gyration. For accurate computation of volumes one should use the hydrodynamic radius instead of R_G. Because $V \sim a^3 N$ where a is a characteristic length (approximately the distance separating two consecutive nucleotides) it follows that $R_G \sim aN^{1/3}$. This general result was first derived by Flory who showed that $R_G \sim aN^{\nu}$ where $\nu = 1/3$ for maximally compact structures. Because RNA is a polyelectrolyte its R_G depends on the concentration of counterions (C). At low values of C, RNA is expanded and the transition to a compact structure occurs only when C exceeds a critical value.

We calculated R_G, using Eq.1 (see Methods), for the 1155 "folded" RNA structures. A plot of R_G as a function of N confirms the Flory result. From the plot in Fig.2(a) we find that, for the folded RNA structures, R_G can be accurately calculated using

$$R_G = aN^{1/3} \tag{7}$$

where $a = 5.5$Å. The prefactor, $a = 5.5$Å, for the folded structures approximately corresponds to the average distance (≈5.5Å) between the phosphate groups along the backbone (Fig.2(b)). Recent measurement of R_G for the compact state of the 195 nucleotides *Azoarcus* ribozyme at high concentration of Na^+ or Mg^{2+} shows that $R_G \approx 35$Å.[9] From Eq.7 we find $R_G \approx 32$Å. This analysis further suggests that the prefactor in Eq.7 may indeed be interpreted as the mean distance between consecutive phosphate groups in the folded structures. If the R_G data in Fig.2(a) for $N < 20$ is neglected we find that Eq.7 is obeyed with $a \approx 5$Å. Thus, the scaling relation is robust.

It is perhaps more reasonable to view RNA structures as formed from relatively rigid duplexes that are linked by flexible motifs such as bulges, loops, etc. In such a picture the fraction of base-paired nucleotides can be chosen as a variable to describe the overall size. We have shown previously (see Fig. 10 in[24]) that the number of base pairs in RNA is $\propto$ N. Thus, the Flory result would be valid even if one accounts for the rigidity of RNA duplexes.

Single-chain RNAs are aspherical and prolate : Even though folded RNA structures are compact, as assessed by their size, there are substantial deviations from sphericity. Indeed, the distribution $P(\Delta)$ for single chain RNAs (Fig.3-(a)) has a broad peak around $\Delta \approx 0.3$. This shows that the native-state conformations of single chain RNA molecules deviate greatly from a sphere. This finding is in stark contrast to $P(\Delta)$ in single-chain protein structures where the peak of the distribution is at $\Delta < 0.1$.[25] In addition, only ∼15% of single-chain RNA structures have $\Delta < 0.2$, while in proteins the corresponding number is ∼80%. This analysis shows that even if native structures of RNAs are compact ($R_G = 5.5N^{1/3}$Å) they are highly aspherical.

Because many RNAs are organized as oligomers, we also obtained the values of Δ for such structures. The distribution of Δ for oligomeric RNAs is also very broad (Fig.3-(a) middle panel). Approximately 34% of the 518 oligomeric RNAs have $\Delta < 0.2$ which shows that oligomerization in RNA increases the sphericity of the molecule. This conclusion is substantiated by analyzing the R_Δ[25] which is the ratio between the degree of asphericity of the oligomer and the average ashpericity of the individual chains. If $R_\Delta = 1$ then the oligmers and the chains have the same asphericity while $R_\Delta < 1$ indicates that the oligomer is more spherical than its components. Nearly ∼60% of oligomeric RNAs have $R_\Delta \leq 1$.

The distribution of the shape parameter, S, in single-chain RNAs (Fig.3-(b) top panel) shows that RNA is mostly prolate because most of the chains have $S > 0$. This tendency towards prolate shapes is stronger than in proteins where ∼50% of single-chains are spherical or nearly so.[25] On the other hand, the complexes of RNA chains found in the PDB structures exhibit a bias towards spherical structures as shown in the peak around $S = 0$ in Fig.3-(b) bottom panel. It should be emphasized that there is no systematic dependence of Δ or S on N. A plot of Δ and S on N shows no correlation whatsoever. The observed variations is directly attributable to sequence and hence the topology of the folded structure.

Distribution function of radius of gyration can be described by WLC model: For the database of RNA molecules, we calculated the distance distribution, $P(r)$, using the coordinates of the heavy atoms. The $P(r)$ functions (Fig.4(a)) for a few RNA molecules, resemble those obtained using SAXS experiments for compact RNA molecules. The value of the persistence length is obtained by fitting $P(r)$ to Eq.6 in the range $R_G < r < 2.5R_G$. As can be seen from Fig.5 the value of l_p varies between (5-25)Å.

If the WLC model correctly describes the distance distribution function an important prediction follows from Eq.6, namely, that by replacing r by the dimensionless variable $x = rl_p/R_G^2$ all the $P(r)$ curves must coincide for $r/R_G > 1$. In other words, irrespective of the

size, sequence or the nature of interactions that stabilize the native topology, the tail of $P(r)$ ($r > R_G$) should superimpose. Thus, $P(r)$ *should be a function of only* $l_p r/R_G^2$. This important prediction is validated in Fig.4(b) in which a plot of $P(x)$ with $x = rl_p/R_G^2$ shows that all the structures follow the same functional form for $x > 0.5$ (see[26] for the same analysis performed on the end-to-end distance distribution of DNA). From this result we conclude that the distance distribution function of RNA structures are well described by the WLC model. We do not have any structural basis for this observation.

Persistence length increases with N: It is remarkable that $P(r)$ for folded RNA is well described by the WLC model which accounts only for the bending penalty of a thin elastic material. The structural basis for this important finding is not clear. By fitting $P(r)$ to Eq.6 for $r/R_G > 1$ we find that l_p for folded structures increases with N. The finding that l_p grows as $l_p = 1.5N^{\alpha}$ with $\alpha \approx 1/3$ can be rationalized using the arguments given below. A consequence of the sublinear growth of l_p with N is that the effective contour length for folded RNA must also grow sublinearly with N, i.e., $L_{eff} = 3 \times \left(\frac{5.5^2}{1.5}\right) N^{1/3} \approx 60N^{1/3}$Å. In the unfolded state we expect the contour length $L \propto N$. Interestingly, recent single molecular measurements have also shown that l_p for microtubules depends on the contour length.[27]

The increase in l_p with N is related to the restriction that the folded states of biomolecules be conformationally less dynamic than unfolded states. It is known from polymer physics that if l_p is fixed and there are no interactions that stabilize a specific structure then on large scales ($\gg l_p$) the structure would be intrinsically flexible. This would mean that spontaneous global fluctuations of folded RNA would be highly likely due to increase in conformational entropy. The requirement that biomolecules should adopt a near unique native fold which minimizes entropy in the native basin of attraction (NBA), implies that l_p itself should grow with N. In contrast, for unfolded RNA, whose conformational entropy is greater than the structures in the NBA, we expect that l_p should be independent of N (see Appendix).

The persistence length l_p, which determines the flexibility of RNA, depends on the concentration, shape, and size of counterions. The balance of the effective energetics of interactions (stacking interactions, hydrogen bonding, hydrophobic interaction, and repulsion between phosphate groups and tertiary interactions) renormalizes l_p. Let us assume that the interactions are approximated as pairwise additive and short-ranged $\Delta G \approx \sum_{|\vec{r}_i - \vec{r}_j| < R_G} \Delta G_{ij}$. In the presence of these interactions the persistence length should scale as the range of the interactions i.e., $l_p \approx R_G \approx N^{1/3}$. The non-local interactions, which stabilize the folded RNA structures, grow with N and hence affect l_p. In the absence of interactions that stabilize the three dimensional

fold l_p is determined only by the intrinsic property of primary sequence and hence should not depend on N (see Appendix).

We further rationalize the dependence of l_p on N by noting that about 54% of all nucleotides in folded RNA structures are involved in base pairing (see Fig. 10 in[24]). One possible way, independent of N, of achieving the 54% base pairings is to distribute them over several short duplexes that are stabilized by tertiary interactions in the native state. Because the tertiary interactions in RNA are weaker than the base stackings (and other) interactions that stabilize hairpin-like structures, creation of several short duplexes is not favorable. Alternatively, it is free energetically more favorable to create a smaller number of longer stable rigid duplexes that are stabilized by tertiary interactions to create a nearly spherical shape. This strategy seems to operate as N increases as seen in ribosomes. As a consequence of the presence of large number of rigid duplexes, which reflects the hierarchical nature of RNA assembly, l_p increases with N. In other words, in RNA there is clear separation in energy scales stabilizing secondary and tertiary interactions. Such a hierarchy implies that stiffness itself must be dependent on N. Because such clear separation in structural organization does not exist in proteins we expect that l_p in proteins must weaker dependence on N (Fig. 5). A similar reasoning has been give to explain the growth of l_p with N for microtubules.[27]

DISCUSSION

Differences in shapes and packing between proteins and RNA: It is difficult to compare, in absolute terms, packing in proteins and RNA because the nature of interactions that stabilize their native structures are distinct.[28] Nevertheless, the Flory scaling ($R_G \sim aN^{1/3}$) observed in RNA and proteins shows that both are maximally compact. For a given N, the approximate volume of RNA is larger than proteins. The ratio, $V_{RNA}/V_{PROT} \approx (a_{RNA}/a_{PROT})^3 \approx 5.6$ for a fixed N. This suggests that, in all likelihood, RNA is more loosely packed than proteins − a conclusion that is in apparent contradiction with a recent structural analysis.[13] Voss and Gerstein based their conclusion on Voronoi construction to decipher volumes of RNA and specific volume calculations. They concluded that "based on well packed atoms" RNA is more tightly packed than proteins.[13] The inherent arbitrariness in assigning volumes to atoms based on Voronoi tessellation of space and the use of mass in the definition of specific volume obscures packing effects which should be based on sizes of nucleotides alone. The present computations show that, based on volume fraction considerations, RNA is not as compact as proteins as long as N (the number of nucleotides or the number of aminoacids) is fixed.

The observed differences between shapes of RNA and proteins are primarily due to the nature of interactions that stabilize the folded structures of RNA and proteins. Tertiary structure formation in RNA must be preceded by substantial neutralization of the negative charges of phosphate groups. Condensation of counterions that are non-specifically bound results in the residual charge on the phosphate group being less than $\sim -0.1e$ where e is the charge of the electron. However, packing in the resulting tertiary fold is determined not only by interactions involving nucleotides but also by correlations between counterions.[29] The condensation of a large number of counterions needed to neutralize the charges on the phosphate groups results in spatial correlation between them. If the volume excluded by the counterions is large (for example the volume of cobalt hexamine is greater than that of Mg^{2+}) then binding of one counterion prevents another one being spatially adjacent. These counterion-mediated interactions and their correlation also inherently affect packing in RNA. In contrast, packing in the core of proteins is predominantly determined by interactions between hydrophobic side chains and their contacts with the protein backbone. Because of the absence of additional ligands, except in certain cases like heme proteins, dense packing in proteins is easier to achieve.

Shape fluctuations of proteins and RNA in the ribosome: The analysis of shape and flexibility of isolated proteins and RNA gives insight into packing in isolated biomolecules. However, in a vast majority of cases, function requires interactions between two or more components. A prime example is the ribosome, a ribonucleoprotein complex, that plays a central role in protein synthesis.[30,31,32,33] Complexes of both small and large subunits with various antibiotics have revealed the mechanism of the ribosomal machinery for tRNA recognition and protein synthesis.[34,35,36,37] The remarkable three dimensional map of entire ribosome (70S) including three tRNAs and mRNA that shows a snapshot of the translation process, has also been resolved by cryo-EM techniques at 5.5Å resolution.[33] The binding interface between 30S and 50S subunits, tRNA recognition site in 30S subunit, and peptidyl transferase site on 50S subunit are all devoid of the ribosomal proteins. The cavity is formed at the interface between two subunits where three tRNA and a string of mRNA can be accommodated. The structures of ~ 50 ribosomal proteins have also been investigated, giving further insights into the interaction and the assembly process of the ribosome.[38,39]

Comparison of the shapes of the structures in isolation and in the complex allows us to infer if there are large scale shape changes upon complexation. To this end, we analyzed the individual components of the ribosome as well as each structural domain by using the parameters that quantify molecular sizes, shapes, and flexibilities of the individual components. We used the

atomic coordinates from 1GIX (30S subunit composed of 16S rRNA, 3 tRNA, 1 mRNA, and 20 r-proteins) and 1GIY (50S subunit composed of 23S rRNA, 5S rRNA and 22 r-proteins) that form an entire ribosome complex upon combination.[33] The parameters characterizing the structural components of ribosome are summarized in Table.I.

r-RNAs : Each ribosomal RNA (16S, 23S rRNA) can be further decomposed into several structural domains whose folding is autonomous even in the absence of ribosomal proteins.[40,41,42,43] The structural features of individual domains of rRNAs in Fig.6(a), 6(b) are quantified in terms of R_G, Δ, and S, with corresponding regions differently colored in the secondary structure map. Comparison of Δ and S values of rRNA domains (Table.I) with $P(\Delta)$ and $P(S)$ in Fig.3 shows that, except for the 3'm domain of 16S rRNA, the overall shapes of rRNA domains are nearly-spherical and slightly prolate ($0 < S < 0.25$). Thus, no significant difference between the overall shape is found in rRNAs domain in comparison to typical RNA molecules. However, the deviations of R_G from the scaling law (Eq.7), especially for the domains of 23S rRNA, II, IV, V, VI, show that they are more extended in size than normal RNA (Fig.7(a)). We find that the size of the domains in the 16S rRNA, 5', C, 3'M obeys the scaling law (Eq.7).

Because the shape of the fold from each domain is identical to the one assembled in the intact ribosome, the assembly from extended domains must occur by a jigsaw puzzle type matching. The head part of the 16S rRNA, which is crucial for A, P, E, tRNA binding sites is entirely composed of the 3'M domain. The 5' and C domains comprise the body and the platform part, respectively (see[33] for terminology). 3'm domain lies at the interface and interacts with IV-domain of the 23S rRNA when the two subunits dock. After the rRNA domains and r-proteins are assembled to form a functional subunit, 50S subunit is highly spherical ($\Delta = 0.05$, $S = -0.01$). *In contrast, the 30S subunit is aspherical and prolate* ($\Delta = 0.21$, $S = 0.14$). The acquisition of the spherical shape of the entire ribosome ($\Delta = 0.03$, $S = 0.01$) must occur after the folding of two subunits. Comparison of the shape of 30S, 50S, and 70S particles suggests that there is very little alteration in their respective Δ and S values upon complexation. This observation suggests that these domains probably fold prior to assembly.

Despite their large sizes, the 50S and the 70S particles are considerably more spherical than the majority of RNA molecules. The globular nature of the 50S particle and the 70S complex is surprising given that the typical RNA complexes are aspherical. This asphericity, especially for medium-sized RNA, is the result of coaxial stacking of helices found in the secondary structures. The stacking leads to formation of long helices which are expected to be rigid with large values of l_p. The 30S subunit, which is highly aspherical and prolate, fits well with this expectation.

Noller has pointed out that the ribosome is made up of mostly small helices linked by flexible bulges and loops.[44] This observation applies to the 50S subunit (Fig.6(b)). However, large-sized coaxial stackings are dominant in the 16S rRNA, but not in the 23S rRNA. As a result, the 30S subunit is highly aspherical. The 70S complex is highly spherical. The globularity of the 70S arises because the 30S subunit fits precisely (despite its high Δ and S values (see Table.I)) at the interface with the 50S to create a nearly perfect sphere.

r-proteins : Similar quantitative analysis can be performed on the ribosomal proteins. The values of R_G in some r-proteins deviate from the scaling law and the shape is generally more biased to the prolate shape than in the non-ribosomal proteins (Fig.7). Ribosomal proteins are mostly distributed on the back of the interface and the periphery of rRNAs with some of proteins being anchored deep into the crevices of rRNA. The anchoring is accomplished using the long tail of peptide chain composed of positively charged amino acids (ARG, LYS, HIS).[38,39] The unusual topology of r-proteins prompted us to investigate whether or not the r-proteins maintain their shape in isolation. We compared the structure of 16 r-proteins complexed in the ribosome ribosome with the isolated r-protein structures independently determined by X-ray or NMR available in PDB. The structural deviation between the isolated and ribosome-complexed r-proteins is quantified using root mean square deviation (RMSD). The structured domains, like α-helix and β-sheet, are well matched in the isolated protein and in the complex, but the structural deviation is large in the loop and the tail regions of the structure. The structure comparison suggests that the ordered part of the r-protein is at least well conserved in both situations. The disordered tail part is stabilized upon complex formation inside the crevices of rRNA.[38,39]

CONCLUSIONS

In this paper we have shown, by analyzing the available RNA structures, that R_G can be accurately computed using the celebrated Flory law. In contrast to proteins, RNA molecules are considerably more aspherical with the overall shape being prolate. The prolate nature of RNA shapes suggests that their diffusion is intrinsically anisotropic. For a given value of N (the number of nucleotides or amino acids) the persistence length of RNA is considerably larger than proteins. These findings suggest that typically RNA is not nearly as densely packed as proteins even though both are compact in the folded states.

The structural basis for the success of WLC model in quantitatively fitting the distance distribution curves for proteins and RNA is not clear. It has been appreciated for a long

time that elasticity-based models are appropriate for ds-DNA in monovalent counterions. The present findings that $P(r)$ (for $r/R_G > 1$) *for compact RNA and proteins* can be described using polymer models that accounts only for bending energies is surprising. Our work shows that l_p, which is needed to describe interaction between biomolecules, can be accurately obtained using the experimentally measurable $P(r)$. The fit of $P(r)$ to WLC also shows that l_p increases with N. Such an unusual behavior is, perhaps, related to the need to minimize entropic fluctuations in the native state. Suppression of conformational fluctuations in long RNA can achieved by having a small number of long rigid helices that are stabilized by weak tertiary interactions. Despite the success of the polymer-based analysis of RNA structures of varying complexity the microscopic basis for characterizing for folded biomolecules using WLC model remains to be established.

APPENDIX

The observation that the persistence length of RNA in the compact folded states increases as $l_p \approx a_1 N^{0.3}$ with $a_1 \approx 1.5$Å was rationalized in terms of the restricted conformational fluctuations in the native state. A corollary of this interpretation is that l_p should become independent of N (or the sequence) if RNA is in the unfolded state. In this appendix, we adopt an oversimplified model for the unfolded state of RNA to explicitly show that at large ($N > 40$) l_p indeed does not depend on N.

The absence of persistent tertiary structure allows us to describe the polynucleotide chain as a worm-like chain model. Such a coarse-grained description may be an approximate representation of a single stranded chain made up of one nucleotide (for example polyA). To verify how l_p changes as N increases we have performed simulations using WLC which takes into account only the excluded volume interactions between the beads representing the nucleotides. The energy function is

$$H = \sum_{i=1}^{N-1} \frac{k_b}{2}(r_{i,i+1} - a)^2 + \sum_{i=1}^{N-2} k_a(1 - \hat{r}_{i,i+1} \cdot \hat{r}_{i+1,i+2}) + \sum_{i=1}^{N-2} \sum_{j=i+2}^{N} \frac{k_e}{2}(r_{i.j} - a)^2 \Theta(a - r_{i,j}) \quad (8)$$

where $r_{i,j}$, $\hat{r}_{i,j}$ are distance and unit vector between i and j beads, respectively. The first term restricts the extension (or reduction) of bond length around a with $k_b = 2000\epsilon/a^2$ where ϵ is the unit of energy. The second term is the bond angle potential that prohibits significant deviation from the equilibrium value. We assign $k_a = 10\epsilon$. The last term with $k_e = 2000\epsilon/a^2$ takes into account volume exclusion interaction. By construction, the homopolymer WLC cannot form any preferred low energy compact structures.

For this model, whose energy function is given by Eq.8, we obtained the end-to-end distance (R_E) distribution function using Monte Carlo simulations. Using the energy function in Eq.8, we generated a large number of equilibrium conformations of the WLC model by employing the pivot algorithm.[45] Unlike a standard Monte Carlo methods that generates polymer conformations by moving each monomer the pivot algorithm produces a global change in the configuration by pivoting the chain around the randomly selected monomer position at each iteration. The algorithm enhances the sampling rate of the available conformational space. The acceptance is judged by Metropolis criterion.

From the ensemble of conformations generated using the pivot algorithm we obtained the end-to-end distribution function $P(R_E)$. The simulated distribution function $P(R_E)$ can be fit using Eq.5 from which we obtain l_p. The dependence of l_p on N for the WLC, without the possibility of forming ordered structures, shows (Fig.8) that l_p becomes independent of N when $N > 40$. The rise in l_p for $N < 40$ is due to the domination of the bending energy (second term in Eq.8). For larger values of N the entropic contributions can compensate for the bending energy and l_p saturates to its intrinsic value. Thus, for WLC with excluded volume interactions the bending penalty dominates at small N values and the chain is intrinsically flexible when N is very large. This situation is in stark contrast with folded RNA (or proteins) where l_p grows with N. The increase of l_p as N increases, which is due to interactions that stabilize RNA, is required to suppress conformational fluctuations when biomolecules reach the functionally competent state. Similar findings are well known for polypeptides such as polyPro, polyGly, etc.[46]

ACKNOWLEDGMENT

This work was supported in part by a grant from the National Science Foundation through NSF CHE-05-14056.

---

[1] Richards, F. M. and Lim, W. A. An anlysis of packing in the protein-folding problem. *Q. Rev. Biophys.* **26**, 423–498 (1994).

[2] Richards, F. M. The interpretation of protein structures: Total volume, group volume distributions and packing density. *J. Mol. Biol.* **82**, 1–14 (1974).

[3] Finney, J. L. Volume occupation, environment and accessibility in proteins. The problem of the protein surface. *J. Mol. Biol.* **96**, 721–732 (1975).

[4] Liang, J. and Dill, K. A. Are proteins well-packed? *Biophys. J.* **81**, 751–766 (2001).

[5] Zuker, M., Mathews, D., and Turner, D. *Algorithms and Thermodynamics for RNA Secondary Structure Prediction: A Practical Guide in RNA Biochemistry and Biotechnology.* Kluwer Academic Publishers, (1999).

[6] Hofacker, I. V. Vienna RNA secondary structure server. *Nucl. Acids. Res.* **31**(13), 3429–3431 (2003).

[7] Gutell, R. R., Lee, J. C., and Cannone, J. J. The accuracy of ribosomal RNA comparative structure models. *Curr. Opin. Struct. Biol.* **12**, 301–310 (2002).

[8] Berman, H. M., Westbrook, J., Feng, Z., Gilliland, G., Bhat, T. N., Weissig, H., Shindyalov, I. N., and Bourne, P. E. The Protein Data Bank. *Nucleic Acids Research* **28**, 235–242 (2000).

[9] Caliskan, G., Hyeon, C., Perez-Salas, U., Briber, R. M., Woodson, S. A., and Thirumalai, D. Persistence Length Changes Dramatically as RNA Folds. *Phys. Rev. Lett.* **95**, 268303 (2005).

[10] Bustamante, C., Marko, J. F., Siggia, E. D., and Smith, S. Entropic elasticity of λ-phase DNA. *Science* **265**(5178), 1599–1600 (1994).

[11] Aronovitz, J. A. and Nelson, D. R. Universal features of polymer shapes. *J. Phys. (Paris)* **47**, 1445–1456 (1986).

[12] Honeycutt, J. D. and Thirumalai, D. Static properties of polymer chains in porous media. *J. Chem. Phys.* **90**, 4542–4559 (1989).

[13] Voss, N. R. and Gerstein, M. Calculation of standard atomic volumes for RNA and comparison with proteins: RNA is packed more tightly. *J. Mol. Biol.* **346**, 477–492 (2005).

[14] Smith, S. B., Finzi, L., and Bustamante, C. Direct Mechanical Measurements of the Elasticity of Single DNA Molecules by Using Magnetic Beads. *Science* **258**, 1122–1126 (1992).

[15] Tinland, B., Pluen, A., Sturm, J., and Weill, G. Persistence Length of Single-Stranded DNA. *Macromolecules* **30**, 5763 (1997).

[16] Liphardt, J., Onoa, B., Smith, S. B., Tinoco, Jr., I., and Bustamante, C. Reversible unfolding of single RNA molecules by mechanical force. *Science* **292**, 733–737 (2001).

[17] Thirumalai, D. and Ha, B.-Y. *Theoretical and Mathematical Models in Polymer Research*, chapter I. Statistical Mechanics of Semiflexible Chains: A Mean Field Variational Approach, 1–35. Academic Press, San Diego (1998). edited by A. Grosberg.

[18] Hyeon, C. and Thirumalai, D. Kinetics of interior loop formation in semiflexible chains. *J. Chem. Phys.* **124**, 104905 (2006).

[19] Wilhelm, J. and Frey, E. Radial Distribution Function of Semiflexible Polymers. *Phys. Rev. Lett.* **77**(12), 2581–2584 (1996).

[20] Fang, X., Littrell, K., Yang, X., Henderson, S. J., Siefert, S., Thiyagarajan, P., Pan, T., and Sosnick, T. R. Mg^{2+}-Dependent Compaction and Folding of Yeast $tRNA^{Phe}$ and the Catalytic Domain of the *B. subtilis* RNase P RNA Determined by Small-Angle X-ray Scattering. *Biochemistry* **39**, 11107–11113 (2000).

[21] Russell, R., Millett, I. S., Doniach, S., and Herschlag, D. Small angle X-ray scattering reveals a compact intermediate in RNA folding. *Nature Struct. Biol.* **7**(5), 367–370 (2000).

[22] Russell, R., Millett, I. S., Tate, M. W., Kwok, L. W., Nakatani, B., Gruner, S. M., Mochrie, S. G. J., Pande, V., Doniach, S., Herschlag, D., and Pollack, L. Rapid compaction during RNA folding. *Proc. Natl. Acad. Sci.* **99**(7), 4266–4271 (2002).

[23] Sleutels, F., Zwart, R., and Barlow, D. P. The non-codeing Air RNA is required for silencing autosomal imprinted genes. *Nature* **415**, 810–813 (2002).

[24] Dima, R. I., Hyeon, C., and Thirumalai, D. Extracting stacking interaction parameters for RNA from the data set of native structures. *J. Mol. Biol.* **347**, 53–69 (2005).

[25] Dima, R. I. and Thirumalai, D. Asymmetry in the shapes of folded and denatured states of proteins. *J. Phys. Chem. B* **108**, 6564–6570 (2004).

[26] Valle, F., Favre, M., de Los Rios, P., Rosa, A., and Dietler, G. Scaling exponents and probability distribution of dna end-to-end distance. *Phys. Rev. Lett.* **95**, 158105 (2005).

[27] Pampaloni, F., Lattanzi, G., Jons, A., Surrey, T., Frey, E., and Florin, E. L. Thermal fluctuations of grafted microtubules provide evidence of a length-dependent persistence length. *Proc. Natl. Acad. Sci.* **103**, 10248–10253 (2006).

[28] Thirumalai, D. and Hyeon, C. RNA and Protein folding: Common Themes and Variations. *Biochemistry* **44**(13), 4957–4970 (2005).

[29] Koculi, E., Lee, N., Thirumalai, D., and Woodson, S. A. Folding of the *Tetrahymena* Ribozyme by Polyamines: Importance of Counterion Valence and Size. *J. Mol. Biol.* **341**(1), 27–36 (2004).

[30] Wimberly, B. T., Brodersen, D. E., Clemons Jr., W. M., Morgan-Warren, R. J., Carter, A. P., Vonrhein, C., Hartsch, T., and Ramakrishnan, V. Structure of the 30S ribosomal subunit. *Nature*

407, 327–339 (2000).

[31] Ban, N., Nissen, P., Hansen, J., Moore, P. B., and Steitz, T. A. The complete atomic structure of the large ribosomal subunit at 2.4 Å resolution. *Science* **289**, 905–920 (2000).

[32] Harms, J., Schluenzen, F., Zarivach, R., Bashan, A., Gat, S., Agmon, I., Bartels, H., Franceschi, F., and Yonath, A. High resolution structure of the large ribosomal subunit from a mesophilic eubacterium. *Cell* **107**, 679–688 (2001).

[33] Yusupov, M. M., Yusupova, G. Z., Baucom, A., Lieberman, K., Earnest, T. N., Cate, J. H. D., and Noller, H. F. Crystal structure of the ribosome at 5.5 Å resolution. *Science* **292**, 883–896 (2001).

[34] Brodersen, D. E., Clemons Jr., W. M., Carter, A. P., Morgan-Warren, R., Wimberly, B. T., and Ramakrishnan, V. The structural basis for the action of the antibiotics tetracycline, pactamycin, and hygromycin B on the 30S ribosomal subunit. *Cell* **103**, 1143 (2000).

[35] Carter, A. P., Clemons Jr., W. M., Brodersen, D. E., Morgan-Warren, R. J., Wimberly, B. T., and Ramakrishnan, V. Functional insights from the structure of the 30S ribosomal subunit and its interactions with antibiotics. *Nature* **407**, 340–348 (2000).

[36] Schluenzen, F., Zarivach, R., Harms, J., Bashan, A., Tocilj, A., Albrecht, R., Yonath, A., and Franceshi, F. Structural basis for the interaction of antibiotics with the peptidyl transferase center in eubacteria. *Nature* **413**, 814 (2001).

[37] Hansen, J. L., Ippolito, J. A., Ban, N., Nissen, P., Moore, P. B., and Steitz, T. The structures of four macrolide antibiotics bound to the large ribosomal subunit. *Mol. Cell* **10**, 117 (2002).

[38] Brodersen, D. E., Clemones Jr., W. M., Carter, A. P., Wimberly, B. T., and Ramakrishnan, V. Crystal structure of the 30 S ribosomal subunit from *Thermus thermophilus*: Structure of the proteins and their interactions with 16 S RNA. *J. Mol. Biol.* **316**, 725–768 (2002).

[39] Klein, D. J., Moore, P. B., and Steitz, T. A. The roles of ribosomal proteins in the structure assembly, and evolution of the large ribosomal subunit. *J. Mol. Biol.* **340**, 141–177 (2004).

[40] Egeberg, J., Leffers, H., Christensen, A., Andersen, H., and Garrett, R. A. Structure and accessibility of domain I of *Escherichia coli* 23 S RNA in free RNA, in the L24-RNA complex and in 50 S subunits. *J. Mol. Biol.* **196**, 125–136 (1987).

[41] Leffers, H., Egebjerg, J., Andersen, A., Christensen, T., and Garrett, R. A. Domain VI of *Escherichia coli* 23 S ribosomal RNA Structure, assembly and function. *J. Mol. Biol.* **204**, 507–522 (1988).

[42] Moore, P. B. and Steitz, T. A. The structural basis of large ribosomal subunit function. *Ann. Rev. Biochem* **72**, 813–850 (2003).

[43] Adilakshmi, T., Ramaswamy, P., and Woodson, S. A. Protein-independent Folding pathway of the 16 S rRNA 5' Domain. *J. Mol. Biol.* **351**, 508–519 (2005).

[44] Noller, H. F. RNA Structure: Reading the Ribosome. *Science* **309**, 1508–1514 (2005).

[45] Bishop, M., Clarke, J. H. R., Rey, A., and Freire, J. J. Investigation of the end-to-end vector distribution function for linear polymer in different regimes. *J. Chem. Phys.* **95**, 4589–4592 (1991).

[46] Cantor, C. R. and Schimmel, P. R. *Biophysical Chemistry.* W. H. Freeman and Company, San Francisco, (1979).

[47] Buscaglia, M., Lapidus, L. J., Eaton, W. A., and Hofrichter, J. Effects of Denaturants on the Dynamics of Loop Formation in Polypeptides. *Biophys. J.* **91**, 276–288 (2006).

[48] Sherman, E. and Haran, G. Coil-globule transition in the denatured state of a small protein. *Proc. Natl. Acad. Sci.* **103**, 11539–11543 (2006).

[49] Pettersen, E. F., Goddard, T. D., Huang, C. C., Couch, G. S., Greenblatt, D. M., Meng, E. C., and Ferrin, T. E. UCSF Chimera - A Visualization System for Exploratory Research and Analysis. *J. Comput. Chem.* **25**, 1605–1612 (2004).

TABLE I: Structural features of the ribosome.

		N^a	R_G[Å]^b	Δ^c	S	l_p[Å]^d	RMSD^e[Å]		N	R_G[Å]	Δ	S	l_p[Å]	RMSD[Å]
	70S	9662	86.2	0.03	0.01	27.1	-							
	30S	3915	66.3	0.21	0.14	23.1	-	**50S**	5747	74.3	0.05	-0.01	23.8	-
	16S	1519	65.1	0.28	0.21	22.3	-	23S	2889	66.4	0.02	-0.01	23.6	-
	5'	542	42.8	0.21	0.14	14.9	-	I	557	46.1	0.23	0.20	16.5	-
	C	352	39.8	0.28	0.25	14.4	-	II	736	56.7	0.08	0.00	18.0	-
r-RNA	3'M	484	39.3	0.07	0.01	13.4	-	III	378	35.4	0.18	0.12	12.3	-
	3'm	141	45.1	0.66	1.06	-^{f}	-	IV	343	44.7	0.25	0.25	15.6	-
							-	V	600	56.3	0.26	0.22	19.4	-
							-	VI	275	41.1	0.22	-0.08	13.2	-
								5S	123	32.5	0.45	0.59	10.6	-
	S2	234	19.3	0.24	0.23	6.4	-	L1	224	18.0	0.15	0.09	6.1	5.79
	S3	206	18.3	0.13	0.08	6.1	-	L2	173	19.1	0.21	0.12	6.0	-
	S4	208	17.6	0.15	0.04	5.9	-	L3	191	22.7	0.29	0.28	**7.1**^{g}	-
	S5	150	16.9	0.28	0.29	5.6	1.19	L4	189	25.7	**0.60**	**0.91**	**7.2**	2.90
	S6	101	14.2	0.10	-0.03	4.5	1.17	L5	122	16.9	0.16	0.10	5.7	-
	S7	155	17.5	0.24	0.19	5.6	0.93	L6	164	19.2	0.39	0.45	5.8	2.06
	S8	138	15.5	0.11	0.00	5.0	-	L7	128	18.1	0.43	0.53	5.7	0.62
	S9	127	18.2	0.41	0.50	**21.8**	-	L9	148	25.9	**0.71**	**1.18**	-	2.19
r-protein	S10	98	18.6	**0.67**	**1.08**	**23.1**	-	L11	133	16.7	0.30	0.32	5.4	2.00
	S11	119	15.0	0.22	0.14	4.7	-	L12	128	18.1	0.42	0.52	5.6	0.75
	S12	124	19.9	0.33	0.38	**23.7**	-	L13	117	14.2	0.11	0.02	4.6	-
	S13	125	22.3	0.46	0.56	**7.1**	-	L14	122	13.4	0.09	0.02	4.4	-
	S14	60	13.8	0.44	0.56	3.9	-	L15	84	13.8	0.23	0.21	4.2	-
	S15	88	13.6	0.19	0.08	4.3	3.89	L16	138	17.4	0.43	0.56	5.6	17.7
	S16	83	12.3	0.13	-0.06	3.8	1.88	L18	113	13.5	0.10	-0.01	4.3	1.84
	S17	104	15.5	0.11	0.02	4.9	4.82	L19	52	10.5	0.09	-0.04	3.0	-
	S18	73	12.0	0.08	-0.04	3.6	-	L22	110	16.6	**0.51**	**0.71**	5.3	-
	S19	80	12.7	0.08	-0.02	3.9	3.16	L23	76	11.5	0.08	0.00	3.5	4.27
	S20	99	17.4	**0.64**	**1.02**	5.4	-	L24	110	15.3	0.08	-0.04	4.9	-
	THX	24	7.2	0.26	0.23	-	-	L25	89	12.3	0.05	-0.01	3.9	1.41
								L29	64	12.8	0.43	0.54	-	-
								L30	60	10.4	0.18	0.09	3.0	-

[a] N is the number of nucleotides or aminoacids.

[b] The radius of gyration R_G is calculated using Eq.1.

[c] The shape parameters Δ and S are computed using Eq.3, 4.

[d] l_p is the persistence length.

[e] The root mean square deviation is the extent of structural deviation of the ribosomal proteins in the complex and in isolation.

[f] Persistence length is not reported if the correlation coefficient of nonlinear fitting is less than 0.85.

[g] Unusually large values of the parameters (Δ, $S > 0.6$, and $l_p > 7.0$Å) are given in bold.

FIGURE CAPTIONS

Figure 1: Distribution of RNA structures in the Protein Data Bank (PDB) as a function of chain length, N. The arrows show the N values for 16S and 23S ribosomal RNAs, respectively. The inset shows the same plot for protein structures.

Figure 2: (a) Radius of gyration as a function of N. The straight line is a fit to the data that shows the scaling law $R_G = 5.5N^{0.33}$Å. The correlation coefficient if 0.94. If data for $N > 300$ are neglected we found $R_G = 5.6N^{0.33}$ with a correlation coefficient of 0.92 (fit in green). Data points inside the circle, which deviate significantly from the scaling law, correspond to the structures that are similar to ds-DNA (PDB code: 1H1K). We excluded these structure from the fitting procedure. For comparison the plot of R_G as a function of N for 13704 monomeric proteins are shown in the inset. The linear line corresponds to $R_G = 3.1N^{0.31}$Å with a correlation coefficient of 0.89. (b) Distance distribution of neighboring phosphor atoms along the RNA backbone. The distance, R_{P-P} corresponds to separation of the backbone P atoms between i^{th} and $(i+1)^{th}$ nucleotide where $i = 1, 2, \ldots, (N-1)$.

Figure 3: (a) Distribution of the asphericity parameter Δ for RNA. The top panel corresponds to single chain, the middle represents single chain in a complex, and the bottom panel is for the complex. Large deviation from sphericity is found in RNA. (b) Distribution of shape parameters for RNA. The legend for the three panel is the same as in (a). RNA molecules in general are aspherical and prolate like an American football.

Figure 4: (a) The distance distribution $P(r)$ as a function of r for selected proteins and RNA. We calculated $P(r)$ using the coordinates of the folded structures. The legend at the bottom gives the PDB codes for which $P(r)$s are shown. (b) Dependence of $P(r)$ on the dimensionless variable $x = rl_p/R_G^2$. If RNA and proteins can be modeled as WLC then it follows that, for $x > 1$, $P(x)$ should fall on a single line (See Eq.6) independent of the fold. The tails of $P(x)$ for $P(r)$ in (a) practically collapse onto a single curve. The $\log P(r)/\beta$ distributions between dash lines are plotted as a function of $-\frac{1}{1-x^2}$, which show a nice overlap with the condition, $\frac{\log[P(x)/\beta]}{-1/(1-x^2)} \sim 1$, being satisfied.

Figure 5: Dependence of l_p on the chain length for RNA and proteins. The persistence length l_p was computed by fitting $P(r)$ to Eq.6. The lines correspond to $l_p = 1.47N^{0.33}$Å (RNA) and $l_p = 1.00N^{0.33}$Å (proteins). There is greater dispersion in the data for proteins than for RNA. Indeed, the correlation coefficient in the fit for RNA is 0.98 whereas for proteins it is only 0.79. Nevertheless, the l_p values for proteins are in the range inferred from experiments for both peptides and proteinsI.[47,48]

Figure 6: (a) Structural domains of the 16S rRNA. The corresponding secondary structure at

the center is in the same color. View from interface (left) and back (right) of 16S rRNA assembled by these structural domains (b) Structural domains of the 23S rRNA. The organization of the figure is identical to that of 16S rRNA in (a). The coaxial stackings, are specified as dark lines on the secondary structures. Molecular graphics images were produced using XRNA and UCSF Chimera package.[49]

Figure 7: (a) Radii of gyration (R_G) of the structural domains in 16S (filled circle) and 23S (empty diamond) rRNAs are plotted as a function of N. Red line representing $R_G = 5.5N^{0.33}$ is drawn to show the deviation of rRNA domain from the statistics found in usual RNAs. (b) Plot of R_G against N for ribosomal proteins. Red line represents $R_G = 3.1N^{1/3}$ scaling law found in "normal" globular proteins. Ribosomal proteins (L3, L4, L9, S10, S12, S13, S20) that show a large deviation from the scaling law are explicitly indicated. When the tail part of these proteins are removed, R_G for the r-proteins obey the Flory scaling law (see open red circles).

Figure 8: Persistence length l_p as a function of N for a WLC model described in the Appendix. This model may represent a homopolymeric nucleotide at low salt concentrations. The value of l_p is obtained by fitting the end-to-end distribution functions $P(R_E)$ that were generated by Monte Carlo simulations (see Appendix). An example of $P(R_E)$ as a function of R_E/L for $N = 30$ is shown in the inset. The dependence of l_p in N shows that, for large N, l_p is a constant for a homopolymer chain at low ionic concentration.

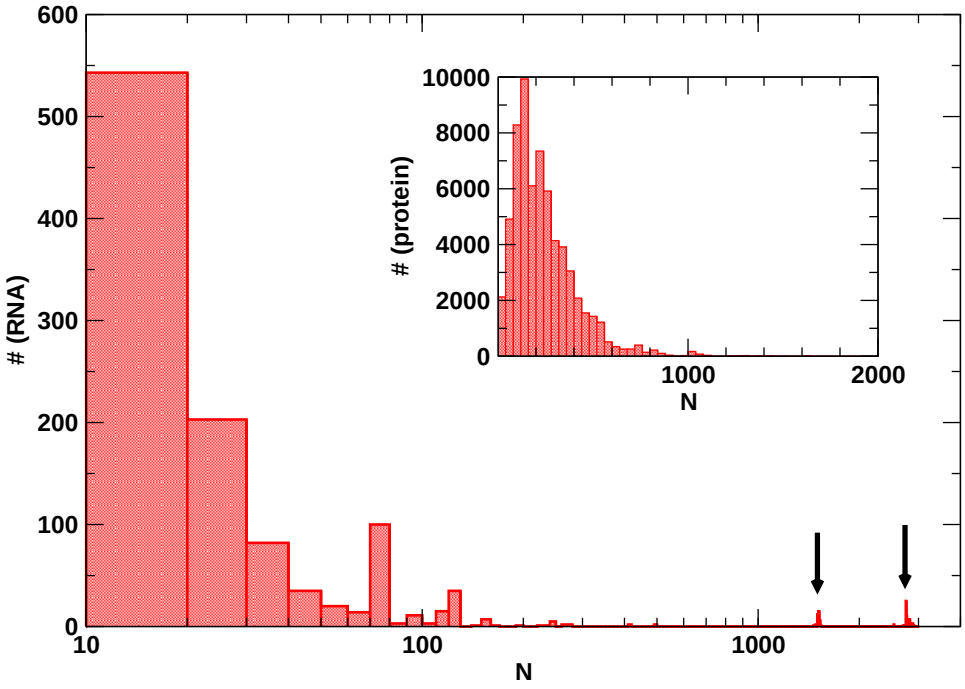
600
500
400
300
200
100
0
(RNA)
10
100
1000
N
10000
8000
6000
4000
2000
0
(protein)
1000
2000
N

FIG. 1:

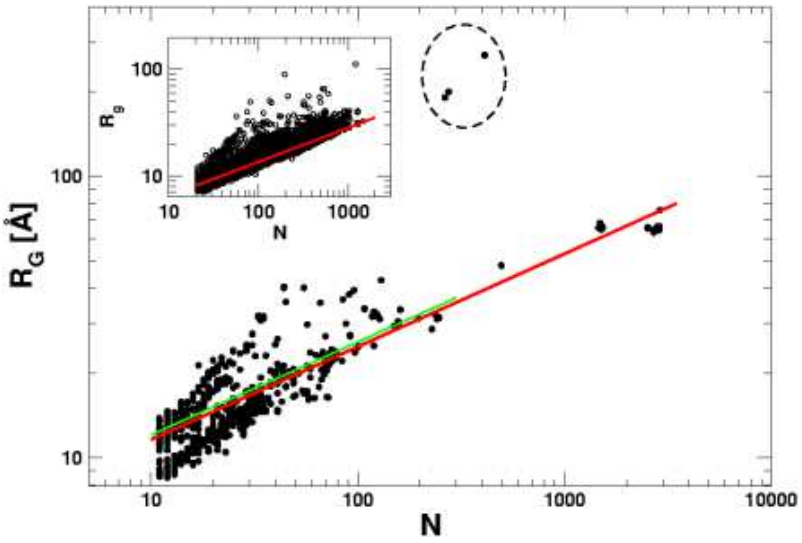

(a)

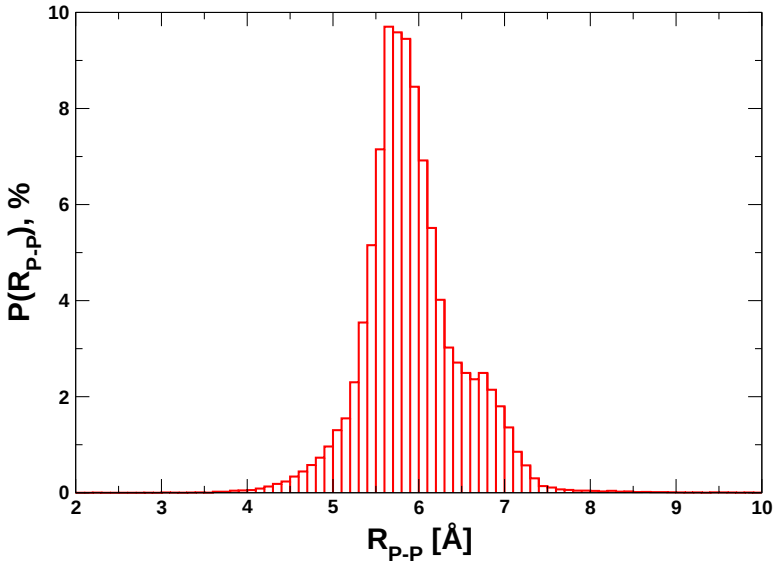

(b)

FIG. 2:

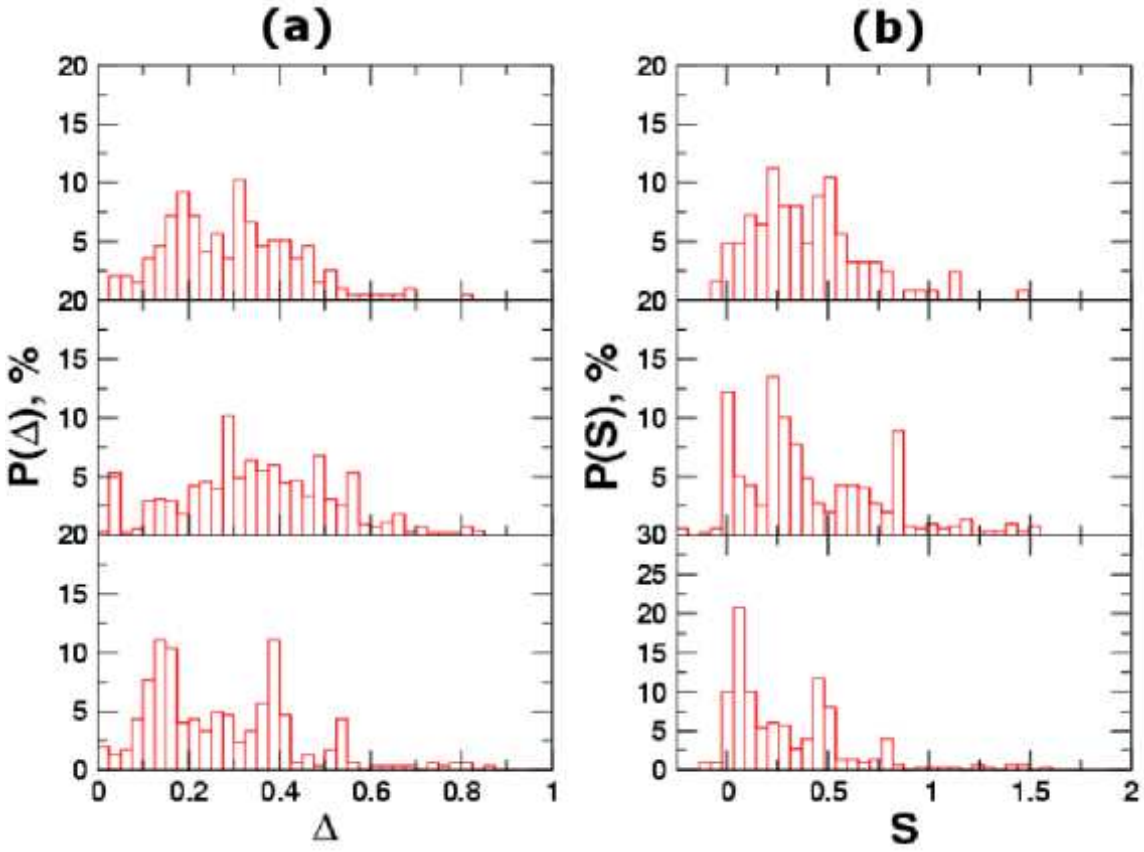

FIG. 3:

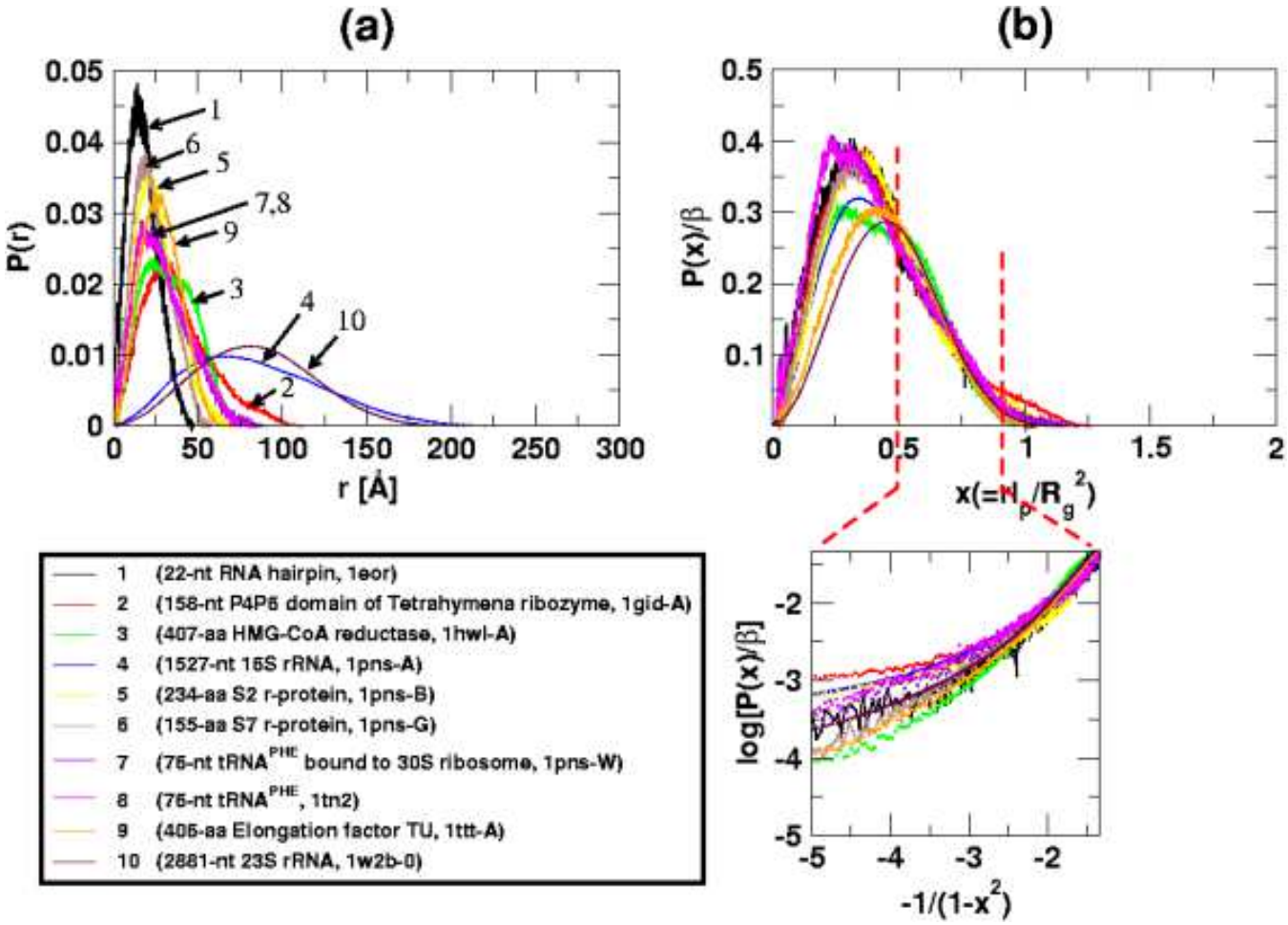
(a)
(b)
P(r)
r [Å]
P(x)/β
x(=R_g^2/R_g^2)
log[P(x)/β]
-1/(1-x^2)
1 (22-nt RNA hairpin, 1eor)
2 (158-nt P4P6 domain of Tetrahymena ribozyme, 1gid-A)
3 (407-aa HMG-CoA reductase, 1hwl-A)
4 (1527-nt 16S rRNA, 1pns-A)
5 (234-aa S2 r-protein, 1pns-B)
6 (155-aa S7 r-protein, 1pns-G)
7 (76-nt tRNA^PHE bound to 30S ribosome, 1pns-W)
8 (76-nt tRNA^PHE, 1tn2)
9 (406-aa Elongation factor TU, 1ttt-A)
10 (2881-nt 23S rRNA, 1w2b-0)

FIG. 4:

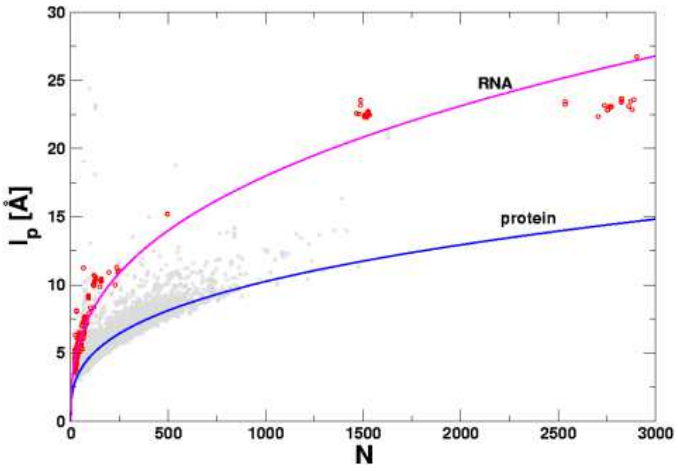
RNA
protein
l_p [Å]
N
0
5
10
15
20
25
30
0
500
1000
1500
2000
2500
3000

FIG. 5:

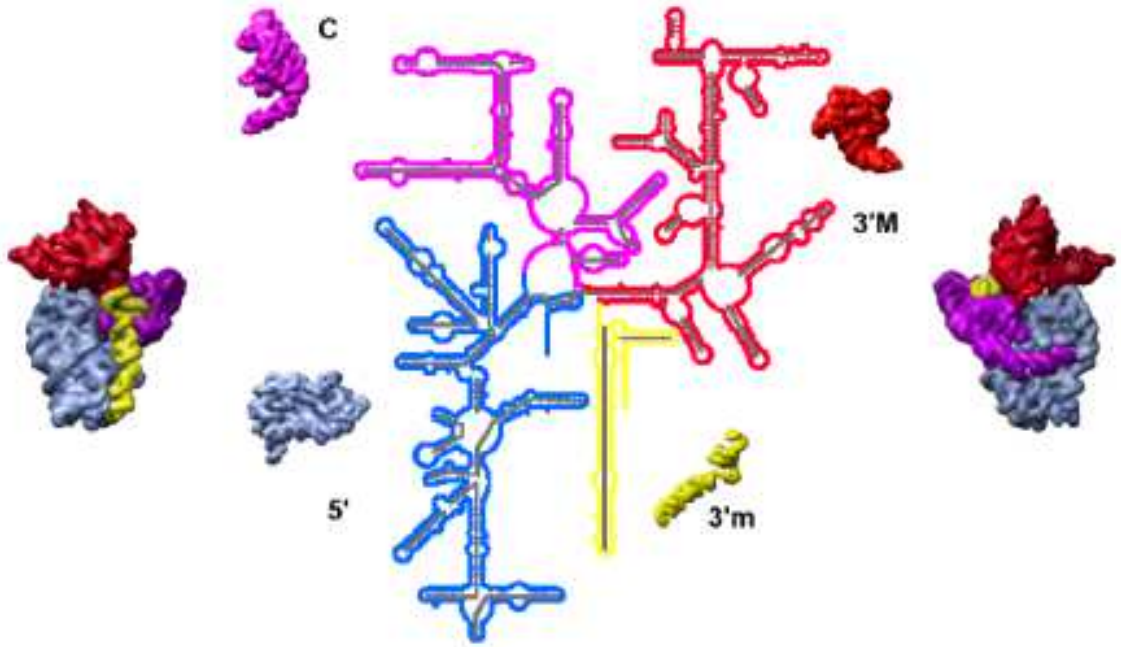

(a)

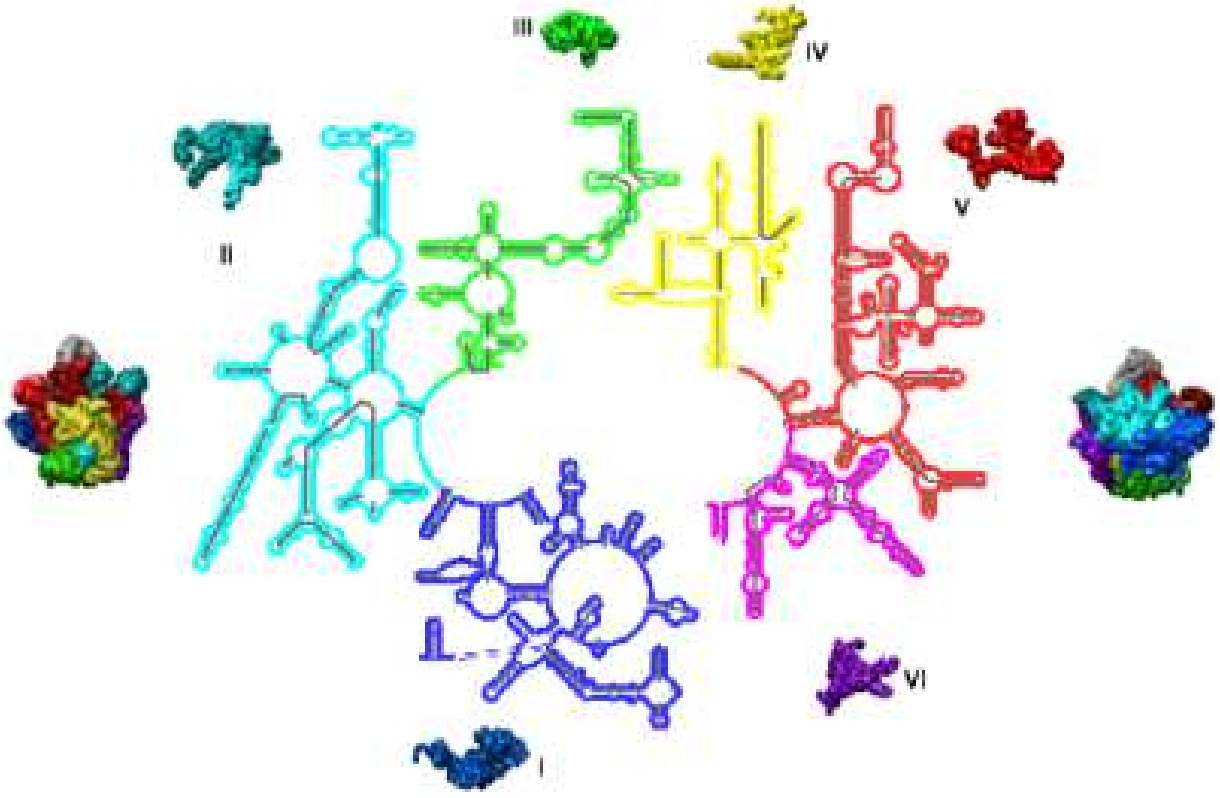

(b)

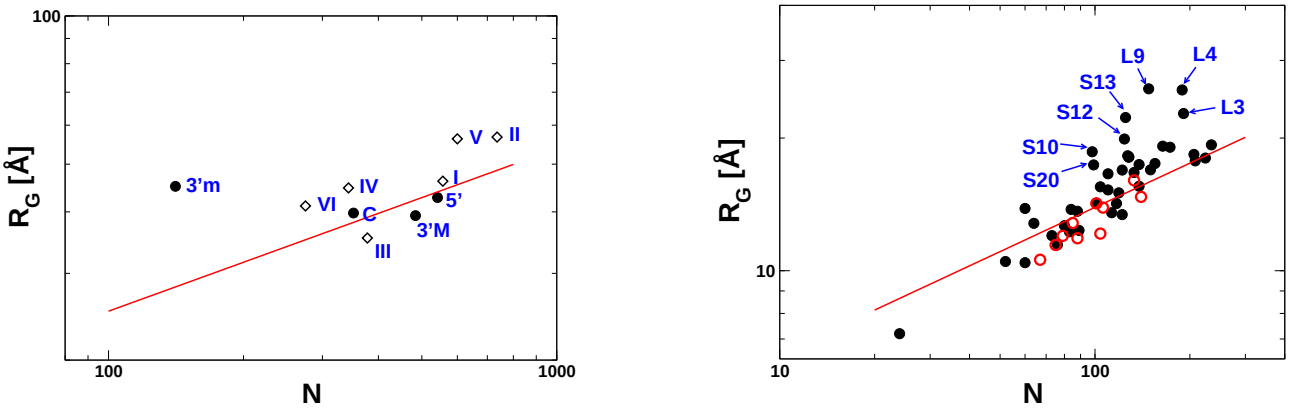
100
R_G [Å]
3'm
VI
IV
C
III
V
II
I
5'
3'M
100
1000
N
L9
L4
S13
L3
S12
S10
S20
10
100

(a) (b)

FIG. 7:

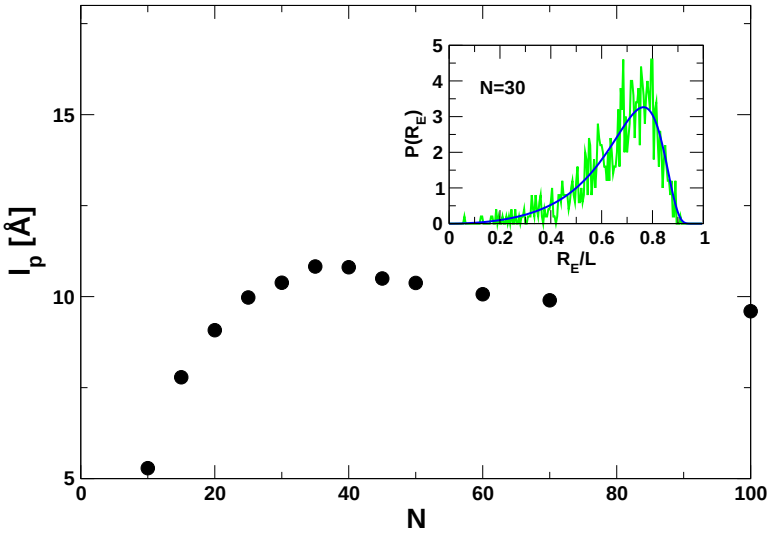
l_p [Å]
15
10
5
0
20
40
60
80
100
N
N=30
$P(R_E)$
0.2
0.4
0.6
0.8
1
R_E/L

FIG. 8: